J Mol Model (2011) 17:857–868
DOI 10.1007/s00894-010-0780-y

ORIGINAL PAPER

Instability of 2,2-di(pyridin-2-yl)acetic acid. Tautomerization *versus* decarboxylation

Piotr Borowski · Ryszard Gawinecki · Anna Miłaczewska · Agnieszka Skotnicka · Krzysztof Woliński · Agnieszka Brzyska

Received: 15 March 2010 / Accepted: 4 June 2010 / Published online: 1 July 2010

Abstract The DFT calculations at the B3LYP level with 6-311G** basis set were carried out in order to reveal whether tautomerization or decarboxylation is responsible for the instability of 2,2-di(pyridin-2-yl)acetic (DPA) and 1,8-diazafluorene-9-carboxylic (DAF) acids. The carboxyl protons in both compounds are involved in the intramolecular hydrogen bonds (the pyridine nitrogen atoms are the hydrogen bond acceptors). Although formation of two intramolecular OH···N hydrogen bonds in the enols of both carboxylic acids enables effective electron delocalization within the quasi rings (···HO−C=C−C=N), only ene-1,1-diol of DAF has somewhat lower energy than DAF itself (ΔE is *ca.* 7 kcal mol^{-1}). DPA and its enediol have comparable energies. Migration of the methine proton toward the carbonyl oxygen atom (to form enediols) requires overstepping the energy barriers of 55-57 kcal mol^{-1} for both DPA and DAF. The enaminone tautomers of the acids, formed by migration of this proton toward the pyridine nitrogen atom, are thermodynamically somewhat more stable than the respective enediols. The energy barriers of these processes are equal to *ca.* 44 and 62 kcal mol^{-1} for DPA and DAF, respectively. Thus, such tautomerization of the acids is not likely to proceed. On the other hand, the distinct energetic effects (*ca.* 15 kcal mol^{-1}) favor decarboxylation. This process involves formation of (*E*)-2-(pyridin-2(1*H*)-ylidenemethyl)pyridine and its cyclic analogue followed by their tautomerization to (dipyridin-2-yl) methane and 1,8-diazafluorene, respectively. Although the later compound was found to be somewhat thermodynamically more stable, kinetic control of tautomerization of the former is more distinct.

Keywords Carboxylic acids · Decarboxylation · DFT calculations · Reaction path · Tautomerization · Transition states

P. Borowski (✉) · A. Miłaczewska · K. Woliński · A. Brzyska
Department of Chemistry, Maria Curie-Skłodowska University,
pl. Marii Curie Skłodowskiej 3,
20-031, Lublin, Poland
e-mail: pibcio@vsop401.umcs.lublin.pl

R. Gawinecki (✉) · A. Skotnicka
Department of Chemistry,
University of Technology and Life Sciences,
Seminaryjna 3,
85-326, Bydgoszcz, Poland
e-mail: gawiner@utp.edu.pl

Introduction

Ene-1,1-diols, often called enols of carboxylic acids, are intermediates in hydration of ketenes [1, 2]: $R_2C=C=O+H_2O \rightarrow R_2C=C(OH)_2 \rightarrow R_2CH-CO_2H$. These compounds are less stable then the corresponding carboxylic acids being energetically favored by delocalization of the lone electron pair of the hydroxy oxygen atom (Fig. 1) [1]. It is known, however, that ene-1,1-diols that contain bulky aromatic groups in the molecule, are more stable [1–4]. The hindered protonation of the β carbon atom in $Ar_2C^{\beta}=C(OH)_2$ caused by *ortho* alkyl groups (Ar=2,4,6-trimethylphenyl, 2,4,6-triisopropylphenyl or 2,3,4,5,6-pentamethylphenyl) is responsible for such a behavior. Enediol of cyclopentadiene-1-carboxylic acid (Fig. 2) was found to be relatively stable [5]. Two intramolecular hydrogen bonds of the resonance-assisted hydrogen bond (RAHB) type [6–9] are expected to be present in its derivative annulated with two pyridine rings (Fig. 3). Unfortunately, neither 1,8-diazafluorene-9-carboxylic (9*H*-cyclopenta[1,2-b;3,4-b′]

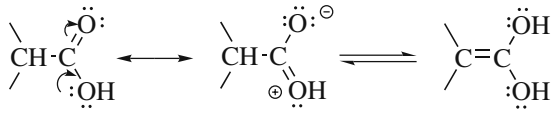

Fig. 1 Relation between carboxylic acids and ene-1,1-diols

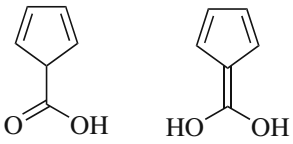

Fig. 2 Cyclopentadiene-1-carboxylic acid and its enol

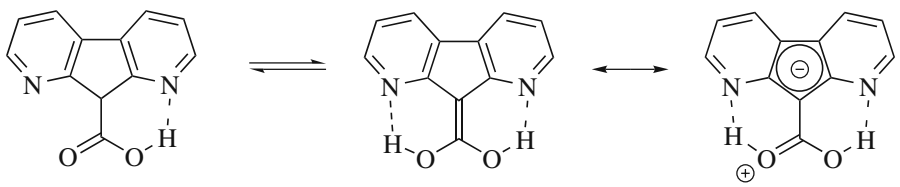

Fig. 3 Relation between 1,8-diazafluorene-9-carboxylic acid and its enol

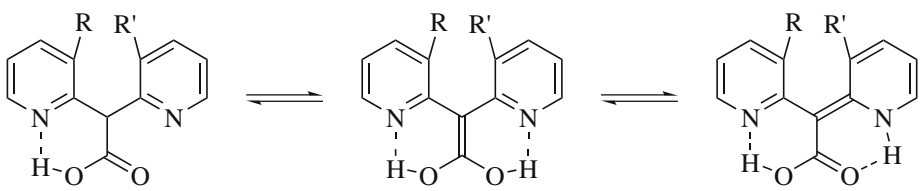

Fig. 4 Relation between 2,2-di(pyridin-2-yl)acetic (R=H) and and 1,8-diazafluorene-9-carboxylic (R=none) acids and its tautomers

dipyridine-9-carboxylic) acid nor its enol are known, but close analogue of the former compound, 2,2-di(pyridin-2-yl) acetic acid, was claimed to be obtained earlier from 2-diazo-1,2-di(pyridin-2-yl)ethanone [10]. Since numerous heterocyclic acetic acids are potentially interesting as anti-arthritic agents [11, 12], the compounds mentioned above seem worthy to be studied from point of view of their stability.

Loosing of the CO_2 molecule by 2- and 4-pyridylacetic acids proceeds smoothly even below 100 °C (this process is much more difficult for 3-pyridylacetic acid) [11–17]. 2-(Pyridin-2- and 4-yl)phenylacetic acids are also exceptionally unstable: benzylpyridines were found to be the only products of the acid hydrolysis of 2-(pyridin-2- and 4-yl) phenylacetonitriles [18]. On the other hand, the enediol and enaminone tautomeric forms of the closely related 2,2-di (pyridin-2-yl)acetic acid (Fig. 4) can be stabilized by two intramolecular hydrogen bonds. Its tendency to decarboxylate is not reported in the only paper devoted to synthesis and properties of this compound [10].

Decarboxylation of carboxylic acid involves formation of carbon dioxide and an organic residue [16]. Organic product is usually stabilized by delocalization of its unshared electron pair. Formation of the intermediate zwitterion $HOCO-C_5H_4N\rightarrow{}^{\ominus}OCO-C_5H_4N^{\oplus}H$ is a common step in the mechanism of enzyme-catalyzed decarboxylations of 2- and 4-pyridylacetic acids [12, 14, 17]. Electron delocalization is particularly important in enzymatic reactions, where an "electron sink" is generally provided by a coenzyme [16].

Despite their instability, the labile compounds may appear as intermediates in numerous (bio)chemical processes. Explanation what are the products these derivatives are transformed to, seems very important. Numerous attempts done in our laboratory to obtain 2,2-di(pyridin-2-yl)acetic acid (**1a**, Fig. 5) from 2-diazo-1,2-di(pyridin-2-yl) ethanone according to the known procedure [10] as well as by hydrolysis of 2,2-di(pyridin-2-yl)acetonitrile (the standard procedure) were unsuccessful. Irrespective of the reason of inaccessibility of this compound to us, its properties can still be discovered by quantum chemical calculations. In the present paper 2,2-di(pyridin-2-yl)acetic (**1a**) and 1,8-diazafluorene-9-carboxylic (**1b**) acids are considered to be susceptible to tautomerization and decarboxylation. The related pyridylacetic acids were used earlier as the models when studying decarboxylation mechanism of aminoacids [19]. It is noteworthy that numerous heterocyclic derivatives of acetic acid are potentially interesting as anti-arthritic agents [20].

Computational details

Density functional theory (DFT, see, *e.g.,* [21]) has been recognized for years to be capable of predicting the very accurate conformations of the covalently bonded systems. Thus, its use in the present paper is justifiable. All calculations were carried out using B3LYP hybrid functional [22, 23] with the 6-311G** basis set [24].

Formulas of 2,2-di(pyridin-2-yl)acetic (**1a**) and 1,8-diazafluorene-9-carboxylic (**1b**) acids, their enol (**2a**,**b**) and enaminone (**3a**,**b**) tautomeric forms as well as the (expected) intermediates (**4a**,**b**) and final products of the decarboxylation process (**5a**,**b**) are depicted in Fig. 5, which also shows numbering of heavy atoms. It should be noted that the carboxyl hydrogen atom H9 (in **1**, **2** and **3**) has the same number even if it is bound to N1 (in **4**) or C7 (in **5**). Formulas of the transition states that are (or may be) formed during decarboxylation of **1a** and **1b** can be seen in Fig. 6. The geometry optimization of all substrates, products and transition states was carried out first. Then, the harmonic frequencies were calculated to establish the types of stationary points, and to find the zero-point energy (ZPE) corrections for the energy barriers and the energetic effects of the processes investigated in the present work. All frequencies for systems **1**–**5(a,b)** were real. On the other hand, one imaginary frequency was found for transition states **TS(1-4) a,b**. Analysis of the eigenvectors corresponding to the imaginary frequencies provided us with the information about the possible products ”on each side” of a transition state at a given stage of the reaction.

Geometry optimization for the transition state is much more complex than for the stable system. This prompted us to carry out some initial, point-wise calculations, corresponding to the so-called distinguished reaction coordinate (DRC). This procedure is not recommended for the accurate description of the reaction path, for example on account of possible discontinuities of energy (and geometrical parameters) as a function of DRC (*i.e.*, some selected geometrical parameter, *e.g.*, bond length). It may, however, provide a reasonable initial structure for which typical algorithms are capable of converging quickly to the required transition state. Therefore, the

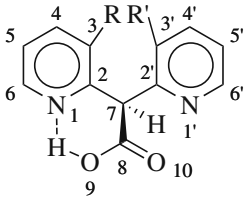

1a, b

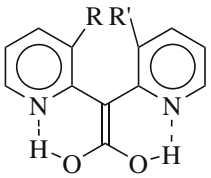

2a, b

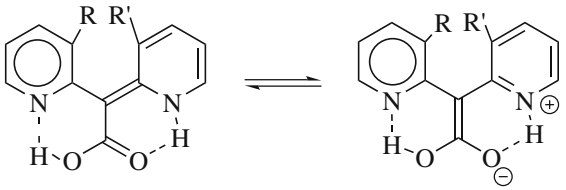

3a, b

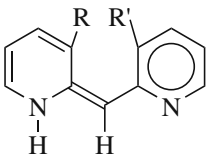

4a, b

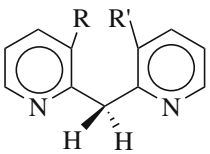

5a, b

R/R' = H/H (**a**) or none (**b**)

Fig. 5 Formulas of the compounds studied and the numbering of the heavy atoms

Fig. 6 Formulas of the transition states studied in this work

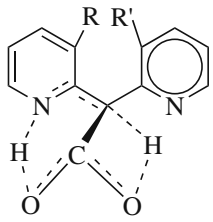

TS1a, b

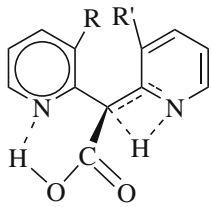

TS2a, b

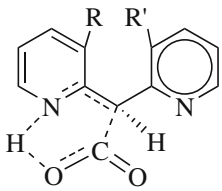

TS3a, b

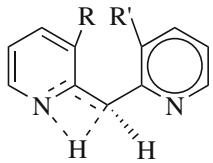

TS4a, b

R/R' = H/H (**a**) or none (**b**)

C7C8 bond was selected as the DRC in reactions **1**→**4**+CO_2. Its length, *R*, was gradually increased from the equilibrium value found for **1** (the applied increment was 0.1 Å), the remaining parameters were optimized, and the geometry corresponding to the highest energy was determined. Since H9 turned out to still be bound to the carboxylic oxygen atom, it was placed in the middle of the O9···N1 distance prior to running the transition state search. On the other hand, the two internal coordinates r_1=H9N1 and r_2=H9C7 (*cf.* Fig. 5) were selected for the description of the proton migration in the **4**→**5** tautomerization. Energies of structures optimized for the remaining geometrical parameters were then computed at a grid of selected linearly independent points. Then, the cross-section of PES (see Fig. 7 for an example), approximated by the 3[rd] degree polynomial, was subjected to straightforward search of the saddle point. All initial structures obtained in this way turned out to converge quickly to the corresponding transition states by following (maximizing along) the lowest (negative) Hessian eigenmode. In order to follow the reaction paths, concept of the so-called intrinsic reaction coordinate (IRC) [25] in mass-weighted Cartesian coordinates was used. All calculations were carried out with the parallel version of the PQS quantum chemistry package [26, 27].

Results and discussion

Molecular geometries

The optimized structures of carboxylic acids as well as these of the enol and enaminone tautomeric forms and products of their decarboxylation (dipyridyl-2-ylmethane and its 1,2-dihydro tautomeric form) are depicted in Fig. 8. Their most important geometrical parameters, as well as geometrical parameters of the transition states **TS(1-4)a,b** are presented in Tables 1 and 2.

The most significant conclusions regarding the molecular geometries are as follow:

1. Arrangement of the N1 and N1′ atoms in the most stable conformer of 2,2-di(pyridin-2-yl)acetic acid **1a** is *trans*-like relative to the C2C7C2′ link (Fig. 8). Turning of one pyridine ring in **1a** by *ca.* 90° around the C7C2′ bond increases the energy by only 0.3 kcalmol^{-1}. Linking of the pyridine rings *via* the C3C3′ bond in **1b** prevents their free rotation and makes the molecule rigid. Note that the N1C2C7C2′ and N1′C2′C7C2 torsion angles in **1b** are close to 180°, *i.e.*, the pyridine rings in the molecule are nearly coplanar. The hydroxyl

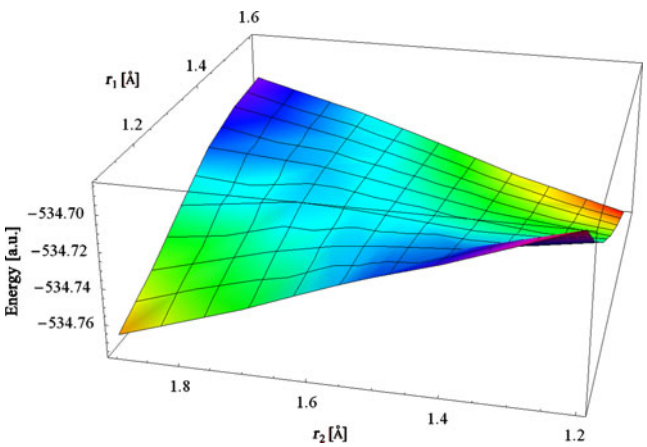

Fig. 7 The cross-section of the potential energy surface (PES) corresponding to the proton migration in **4a**→**5a** reaction (see text for the definition of the internal coordinates)

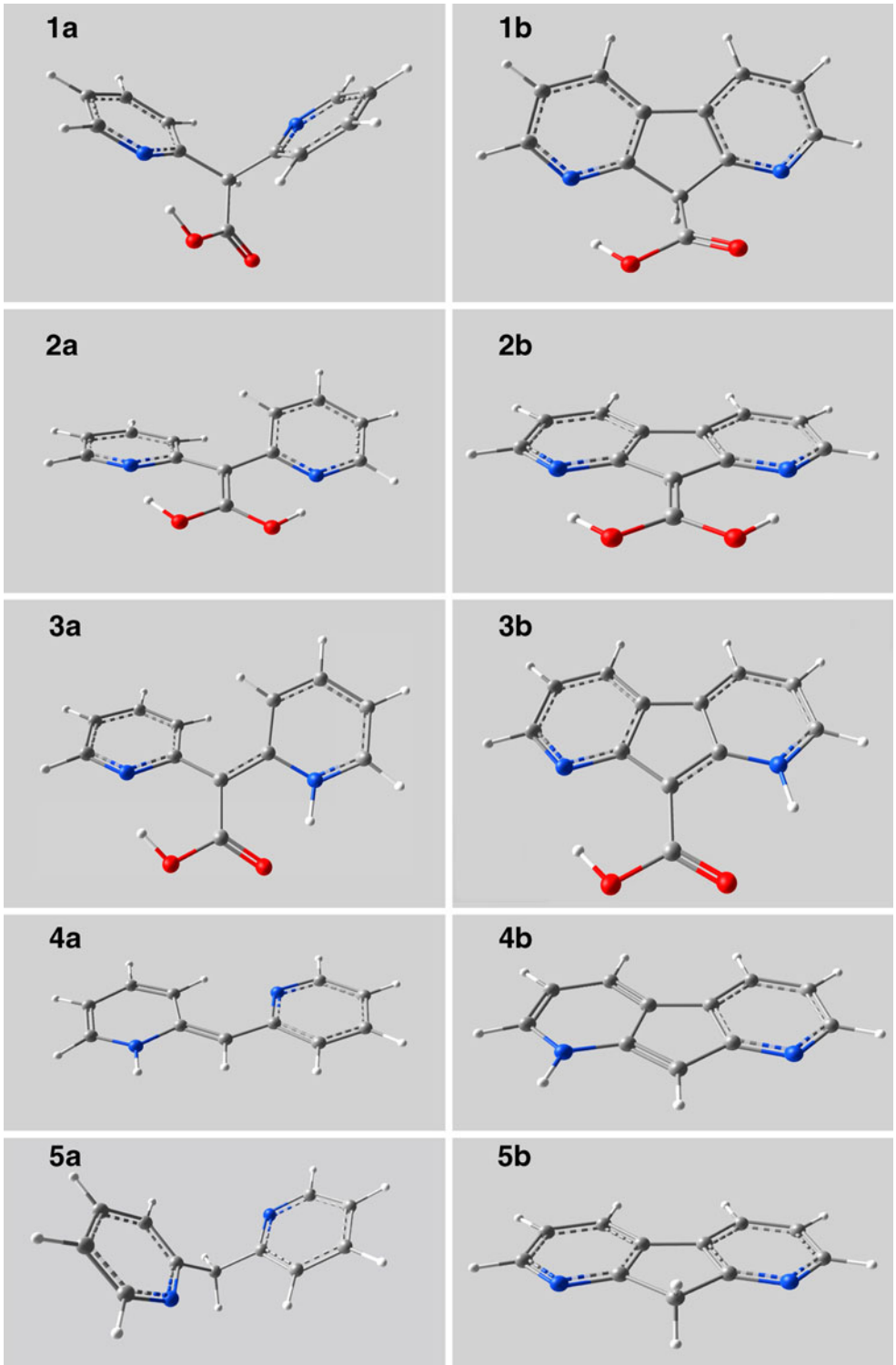

Fig. 8 Optimized structures of the substrates and products of the tautomerization/decarboxylation processes

groups both in **1a** and **1b** are involved in the intramolecular hydrogen bond with the N1 atom being the hydrogen bond acceptor. The OH bond in **1a** is somewhat longer than 0.99 Å (a typical OH bond length in the dimers of ordinary carboxylic acids where very strong intermolecular hydrogen bonds are present). On the other hand, the OH bond in **1b** is shorter (*ca.* 0.98 Å). Rigidity of the **1b** molecule and, consequently, steeper

Table 1 Selected optimized (B3LYP/6-311G**) bond lengths [Å] as well as valence and torsion angles [deg] in compounds **1-5**

Bond/angle	1a	1b	2a	2b	3a	3b	4a	4b	5a	5b
O9H9	0.993	0.981	1.021	0.990	1.000	0.981	–	–	–	–
N1H9	1.738	1.918	1.572	1.965	1.654	2.005	1.009	1.009	–	–
O10H7	–	–	1.021	0.990	1.606	2.138	–	–	–	–
N1′H7	–	–	1.572	1.965	1.047	1.021	–	–	–	–
C8O10	1.201	1.195	1.306	1.315	1.238	1.223	–	–	–	–
C8O9	1.339	1.345	1.306	1.315	1.328	1.344	–	–	–	–
C7H7	1.089	1.098	–	–	–	–	1.087	1.079	1.091	1.095
C7H9	–	–	–	–	–	–	–	–	1.091	1.095
C7C2	1.523	1.513	1.462	1.433	1.467	1.436	1.375	1.372	1.517	1.511
C7C2′	1.534	1.514	1.462	1.433	1.415	1.387	1.444	1.441	1.517	1.511
C7C8	1.546	1.550	1.419	1.376	1.479	1.450	–	–	–	–
N1C2	1.340	1.325	1.359	1.338	1.356	1.341	1.402	1.377	1.340	1.326
N1C6	1.338	1.344	1.336	1.340	1.335	1.336	1.365	1.363	1.337	1.342
N1′C2′	1.338	1.323	1.359	1.338	1.380	1.359	1.355	1.343	1.340	1.326
N1′C6′	1.335	1.341	1.336	1.340	1.350	1.356	1.333	1.334	1.337	1.342
C2C3	1.397	1.407	1.415	1.428	1.414	1.433	1.445	1.469	1.399	1.412
C3C4	1.389	1.391	1.383	1.389	1.384	1.389	1.360	1.367	1.390	1.391
C4C5	1.394	1.396	1.398	1.398	1.396	1.395	1.432	1.423	1.392	1.394
C5C6	1.388	1.393	1.384	1.397	1.387	1.400	1.357	1.368	1.392	1.395
C2′C3′	1.397	1.412	1.415	1.428	1.433	1.449	1.417	1.435	1.399	1.412
C3′C4′	1.391	1.391	1.383	1.389	1.369	1.375	1.382	1.390	1.390	1.391
C4′C5′	1.391	1.393	1.398	1.398	1.417	1.417	1.397	1.391	1.392	1.394
C5′C6′	1.392	1.396	1.384	1.397	1.366	1.375	1.390	1.403	1.392	1.395
C3C3′	–	1.463	–	1.461	–	1.451	–	1.442	–	1.463
C2C7C2′	109.0	101.8	122.8	106.9	121.7	105.9	129.1	106.5	112.1	102.4
C2N1C6	119.3	116.7	120.9	115.8	120.5	116.1	124.9	122.3	118.1	116.2
C2′N1′C6′	118.2	116.1	120.9	115.8	124.9	121.4	118.7	116.0	118.1	116.2
C2C7C8	116.6	113.3	118.6	126.5	120.2	129.8	–	–	–	–
C2′C7C8	111.1	116.9	118.6	126.5	118.1	124.3	–	–	–	–
N1C2C7C8	37.0	-52.0	19.8	0.0	28.0	0.0	–	–	–	–
N1′C2′C7C8	145.2	58.8	19.8	0.0	12.2	0.0	–	–	–	–
N1C2C7C2′	-89.8	178.3	-160.2	180.0	-152.1	180.0	180.0	180.0	-95.8	180.0
N1′C2′C7C2	-85.0	-177.3	-160.2	180.0	-167.7	180.0	0.0	180.0	-95.8	180.0

energy increase along the interring torsional motions, prevent the H9 and N1 atoms to approach each other as close as in **1a**. This results in elongation (weakening) of the H···N1 hydrogen bond (1.918 Å in **1b** *vs.* 1.738 Å in **1a**) and shortening (strengthening) of the O9H bond. The carbon-nitrogen bond lengths in the pyridine rings of **1a** and **1b** are close to these in pyridine itself (1.337 Å; geometry optimized at the B3LYP/6-311G** level). The same applies to the ring carbon-carbon bond lengths which are comparable to the average bond length in pyridine (1.393 Å). Slight elongation of the carbon-nitrogen bonds in **1a** and **1b** is observed for the ring involved in the hydrogen bonding. The valence CNC angles in these systems are also comparable to those found in the molecule of pyridine (117.2°).

2. Formation of the H···N1 and H···N1′ hydrogen bonds in **2a** and **2b** affects the hybridization of C7 and shortens the C7C8 bond lengths (1.419 Å in **2a** and 1.376 Å in **2b**) as compared to these in **1a** and **1b**. These bonds resemble more the carbon-carbon bonds in the benzene ring (~1.39 Å) rather than those in alkenes (~1.33 Å). It should be noted that C7C8 bond in **2a** is longer, while this in **2b** is shorter than 1.39 Å. Effective electron delocalization in the quasi rings that involve OH···N fragments results also in shortening of the C7C2 and C7C2′ bonds both in **2a** and **2b** (they are still significantly longer than the aromatic carbon-carbon

Table 2 Selected optimized (B3LYP/6-311G**) bond lengths [Å] as well as valence and torsion angles [deg] in the transition states

Bond/angle	TS1a	TS1b	TS2a	TS2b	TS3a	TS3b	TS4a	TS4b
O9H9	1.009	0.984	0.994	0.982	1.829	1.549	–	–
N1H9	1.754	2.078	1.721	1.883	1.030	1.093	1.263	1.356
O10H7	1.246	1.345	2.881	2.861	–	–	–	–
N1′H7	2.829	2.596	1.271	1.358	–	–	–	–
C8O10	1.265	1.260	1.216	1.208	1.192	1.204	–	–
C8O9	1.290	1.307	1.338	1.350	1.221	1.262	–	–
C7H7	1.526	1.455	1.583	2.115	1.085	1.093	1.091	1.086
C7H9	2.459	2.464	1.362	2.355	–	–	1.608	1.609
C7C2	1.485	1.456	1.463	1.417	1.432	1.464	1.467	1.435
C7C2′	1.493	1.488	1.490	1.434	1.492	1.499	1.455	1.460
C7C8	1.489	1.452	1.495	1.475	1.951	1.692	–	–
N1C2	1.354	1.336	1.354	1.357	1.371	1.335	1.359	1.343
N1C6	1.337	1.342	1.335	1.322	1.356	1.351	1.343	1.338
N1′C2′	1.345	1.328	1.351	1.427	1.345	1.327	1.353	1.341
N1′C6′	1.335	1.338	1.341	1.344	1.333	1.339	1.335	1.331
C2C3	1.403	1.418	1.413	1.437	1.416	1.411	1.399	1.411
C3C4	1.387	1.391	1.384	1.403	1.374	1.388	1.387	1.399
C4C5	1.395	1.396	1.397	1.381	1.414	1.406	1.405	1.401
C5C6	1.388	1.396	1.387	1.415	1.367	1.383	1.384	1.403
C2′C3′	1.407	1.427	1.390	1.483	1.405	1.422	1.413	1.444
C3′C4′	1.386	1.391	1.392	1.382	1.388	1.391	1.383	1.394
C4′C5′	1.395	1.392	1.399	1.400	1.392	1.392	1.398	1.388
C5′C6′	1.390	1.398	1.386	1.394	1.392	1.398	1.390	1.404
C3C3′	–	1.455	–	1.420	–	1.460	–	1.452
C2C7C2′	117.8	104.6	119.9	105.4	122.7	101.4	121.3	102.0
C2N1C6	119.7	116.0	119.9	116.7	124.1	120.8	123.3	118.4
C2′N1′C6′	118.9	116.2	123.1	115.6	118.8	116.2	118.5	116.5
C2C7C8	113.7	121.0	123.1	127.0	104.2	107.7	–	–
C2′C7C8	112.3	127.7	111.0	127.2	101.7	122.7	–	–
N1C2C7C8	-30.2	10.3	23.2	-5.2	54.7	-41.3	–	–
N1′C2′C7C8	-1.7	-22.8	-95.8	13.2	104.5	62.8	–	–
N1C2C7C2′	104.3	163.7	173.6	-178.8	-59.6	-171.3	138.3	-157.3
N1′C2′C7C2	-136.7	-173.7	110.5	-173.2	-139.9	-177.4	-12.6	-176.9

bonds) as compared to these in **1a** and **1b** (the C7C8, C7C2 and C7C2′ bonds in their molecules are typical carbon-carbon single bonds). The H9O9 and the hydrogen H···N1$^{(\prime)}$ bond lengths in **2a**,**b** follow the same pattern as these in the molecules of **1a**,**b**. Moreover, C3C3′ bond in **2b** is much longer than C7C2$^{(\prime)}$ and C2$^{(\prime)}$C3$^{(\prime)}$ bonds (which have comparable lengths, *cf.* Table 1). Thus, aromaticity of the five membered ring in **2b** is doubtful what negates stabilization of this form by resonance suggested in Fig. 3.

3. The NH···O hydrogen bonds are present in the enaminone tautomeric forms **3a** and **3b** (these bonds are longer than the OH···N hydrogen bonds in **2a** and **2b**). Contribution of the zwitterionic structures of **3** (*cf.* Figure 5) is manifested in shortening of the C7C8 bonds (this effect is not as significant as for **2**) and elongation of the C8O10 bonds as compared to **1**.
4. **4a** and **4b** seem likely to be the intermediate products of decarboxylation of **1a** and **1b**, respectively. Both these molecules are planar. Hydrogen atom involved in the H···N1 hydrogen bonding in **1a** and **1b** is bound to N1. The N1H bond lengths (1.009 Å in both systems) are in between these found for pyrrole (1.006 Å) and aliphatic amines (1.015 Å; geometry optimized at the B3LYP/6-311G** level). The C7C2 and C7C2′ bond lengths are intermediate between these of the single and double carbon-carbon bonds. In both **4a** and **4b** the

C7C2 bonds are shorter, while C7C2′ are longer than 1.39 Å (Table 1).

5. **5a** and **5b** are probably the final products of decarboxylation of **1a** and **1b**. Their geometrical parameters remain similar to these found for **1a** and **1b**, as well as those in pyridine itself. Note that the pyridine rings in **5b** are coplanar.

Reaction paths and energetic effects

Calculations of the energetic effects of the most intuitive reactions **1**→**5**+CO_2 reveal that products are by *ca.* 13.6 (case **a**) and *ca.* 15.8 kcalmol^{-1} (case **b**) more stable than substrates. All energetic effects $|E_{products} - E_{substrates}|$ and energy barriers $E_{TS} - E_{substrates/products}$ discussed (denoted as ΔE) were corrected for the zero-point energy, ZPE. They are depicted in Fig. 9. The data used in order to obtain these values (*i.e.*, total energies of the molecules and ZPE corrections of all stable structures and transition states) are reported in Table 3. Note that for the brevity reason the ΔG values were calculated for decarboxylation processes only. Comparable entropies of the substrates and products for the tautomerization processes suggest that the ΔE and ΔG values also approximate each other.

Ene-1,1-diols **2** have lower energies than the respective acids **1**: the energy lowering is equal to approximately 0.7 and 7 kcalmol^{-1} for **2a** and **2b**, respectively (Fig. 9). The energy barriers for the proton migration from C7 toward the carbonyl oxygen atom O10 (this processes proceed *via* **TS1** transition states) are nearly the same for **a** and **b** and amount to *ca.* 55 kcalmol^{-1}. The enaminone tautomeric forms **3a**,**b** are thermodynamically somewhat more stable than **2a,b** (by nearly 4 kcalmol^{-1} in the case of **3b**). However, the energy barriers for the migration of proton H7 toward N1′, associated with the presence of **TS2a** and **TS2b** transition states, differ significantly: the calculated ΔE values are equal to *ca.* 44 and *ca.* 62 kcalmol^{-1} for **1a**→**3a** and **1b**→**3b**, respectively. In a view of finding more energetically favorable processes from the thermody-

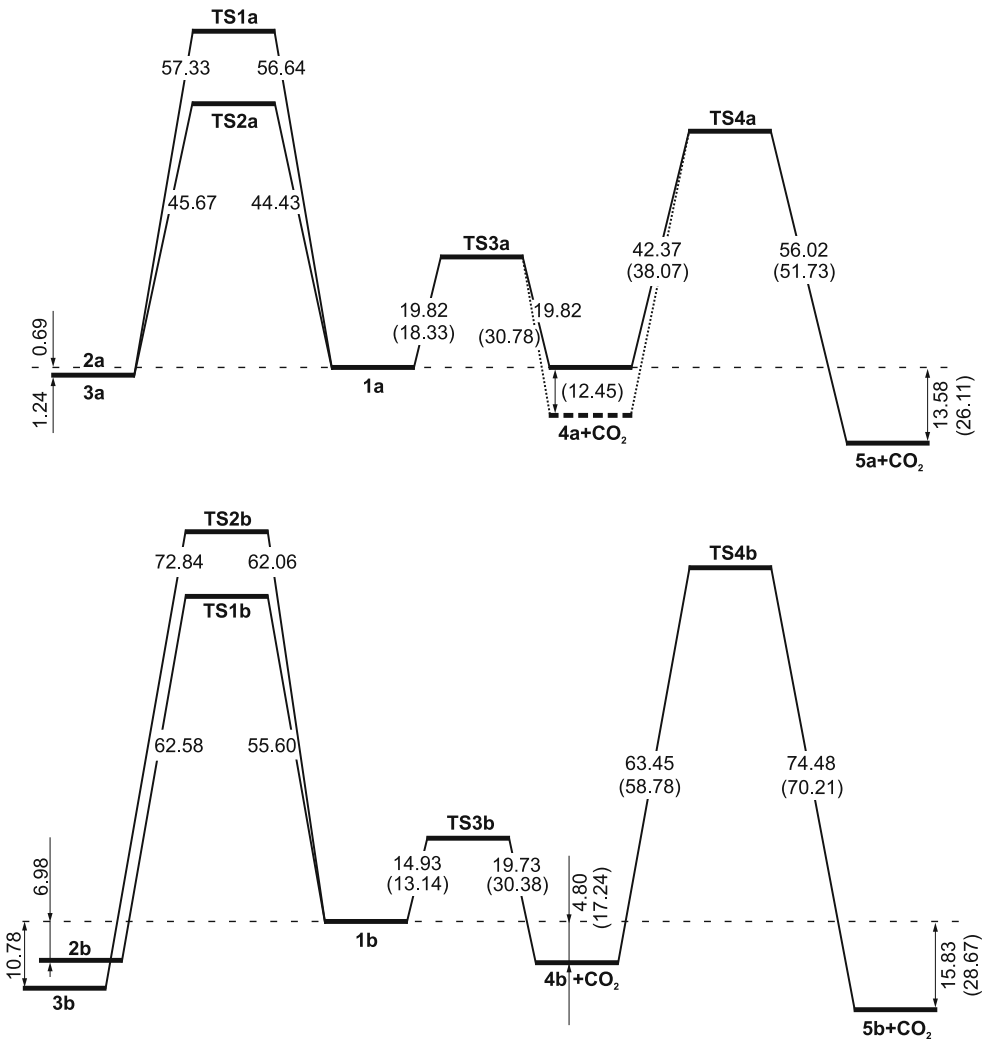

Fig. 9 Reaction paths, ZPE corrected energy barriers and energetic effects (ΔE in kcal mol^{-1}) in tautomerization and decarboxylation of **1a** and **1b**. The calculated ΔG values (for decarboxylation processes only) are reported in parentheses

Table 3 Total energies (in a.u.) and ZPE corrections (in kcal mol^{-1}) of the substrates, products and transition states

	E	ZPE
2a	-723.447573	125.63
3a	-723.449268	126.14
↑		
TS1a	-723.350792	122.21
TS2a	-723.370685	122.49
↓		
1a	-723.447339	126.17
↓		
TS3a	-723.413217	124.57
↓		
4a+CO_2	-723.443569	123.81
↓		
TS4a+CO_2	-723.369568	119.72
↓		
5a+CO_2	-723.465199	123.80
2b	-722.252866	113.08
3b	-722.259203	113.25
↑		
TS1b	-722.146161	108.67
TS2b	-722.135826	108.65
↓		
1b	-722.240663	112.39
↓		
TS3b	-722.213498	110.27
↓		
4b+CO_2	-722.245186	110.43
↓		
TS4b+CO_2	-722.136557	105.69
↓		
5b+CO_2	-722.262235	110.10

namic and kinetic point of view (*vide infra*) we conclude that tautomerization of **1a** and **1b** is not likely to proceed. Among all investigated processes, namely **1**→**2**, **1**→**3**, and **1**→**5**+CO_2, the most distinct energetic effect can be seen for **1**→**5**+CO_2 (for both **a** and **b**, *cf.* Fig. 9). These processes will be discussed in detail.

Rupture of the C7C8 bond in the **1**→**4**+CO_2 reaction is probably followed by migration of the carboxylic hydrogen atom to C7 (this results in formation of **5**). The concerted and step-wise mechanisms have to be considered here. In the first one, the eigenmode (atomic displacements) corresponding to the imaginary frequency should correspond to simultaneous detachment of CO_2 and migration of the carboxylic proton H9 toward C7. The later mechanism is expected to involve a few different transition states. Case **a** will be considered first. A quick glance at the structure of **1a** points at the second, *i.e.*, step-wise mechanism. The reason for this is a significant energy increase when H9 approaches C7, while C7 is still bound to C8. It is shown in Fig. 10 as a steep, violet (turning to blue at larger values of *R*) "slope" on a cross-section of the potential energy hypersurface of **1a**. In addition, elongation of the C7C8 bond reveals that there is a clear trend for the H9 atom to approach N1, *i.e.*, to form **4a**. Therefore one should search for a transition state that appears in the course of reaction **1a**→**TS3a**→**4a**+CO_2. It was found to be nearly 20 kcal mol^{-1} above **1a**. The calculated ΔG value corresponding to the reported ΔE amounts to 18.33 kcal mol^{-1}. This value is known to be low enough for the process that is fast under standard conditions. Analysis of geometrical parameters shows that C7C8 bond in **TS3a** is significantly longer than that in **1a**, and that the H···N1 bond remains close to that of **4a** (*cf.* Tables 1 and 2). The structure of **TS3a** is depicted in Fig. 11 (the eigenmode, corresponding to the imaginary frequency equal to i320cm^{-1}, is also shown there). Following the reaction path from **TS3a** along the intrinsic reaction coordinate (IRC), **1a** or **4a** + CO_2 were obtained. No energy lowering is observed at this stage of decarboxylation. However, value of the Gibbs free energy of the products calculated at 298 K is by more than 12 kcal mol^{-1} lower than that of **1a**. Although rotational and vibrational entropies were also changed (ΔS_{rot}=11.9 cal mol^{-1}K^{-1} and ΔS_{vib}= -12.2 cal mol^{-1}K^{-1}), significant increase in the translational entropy (ΔS_{trans}=36.6 cal mol^{-1}K^{-1}) gives the major contribution to the reported value of ΔG. The low energy barrier being<20 kcal mol^{-1} (corresponding to energy of quanta in the near IR region) as well as negative value of ΔG clearly show that **1a** decomposes spontaneously (and rapidly) to form **4a** and CO_2. This proves that Eistert and Schade [10] could not obtain **1a**. It is probably why we were not able to obtain this compound starting from 2-diazo-1,2-di(pyridin-2-yl)ethanone [10] as well as by hydrolysis of 2,2-di(pyridin-2-yl)acetonitrile (the standard procedure).

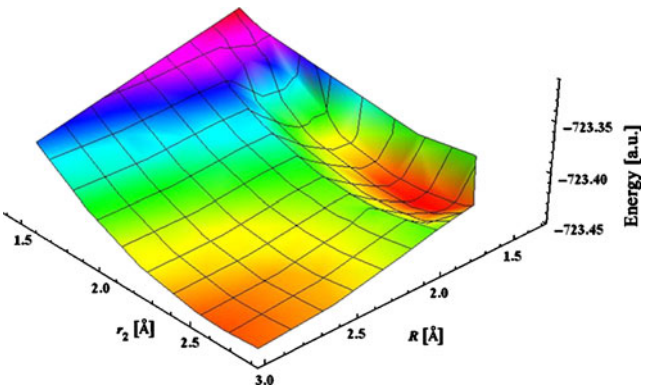

Fig. 10 Cross-section of the potential energy surface (PES) of **1a** corresponding to the rupture of C7C8 (variable *R*) bond and simultaneous migration of the hydroxyl proton toward C7 (variable r_2)

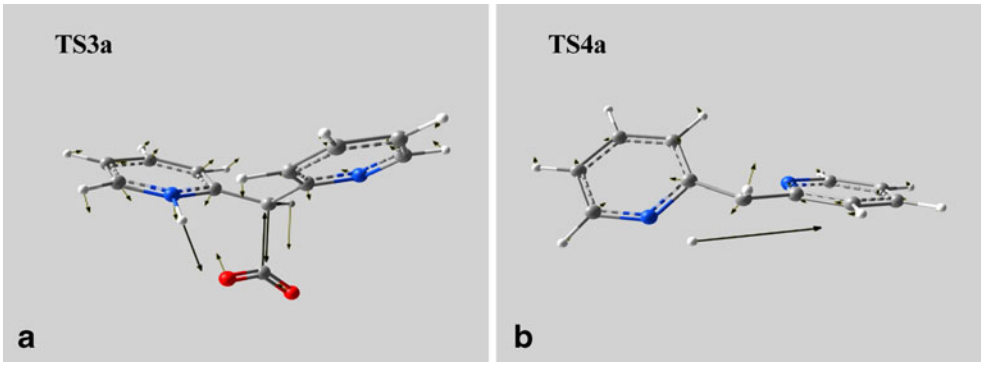

Fig. 11 Transition states **TS3a** and **TS4a**. The arrows show the atomic displacement corresponding to the imaginary frequencies

4a is probably an intermediate in the process of decarboxylation of **1a**. In order to obtain **5a**, which is the most stable system studied (at least at the B3LYP level, *cf.* Fig. 9 and Table 3), the C7H9 bond has to be formed and, at the same time, the N1H9 bond has to be broken. It was not clear to us which is the mechanism of this step (*i.e.*, unimolecular or bimolecular). It was initially assumed that the rearrangement takes place within the single molecule. This process is accompanied by breaking of the planar symmetry of **4a** (note that C7 atom has to change its hybridization from sp^2 in **4a** to sp^3 in **5a**). The search for another transition state (**TS4a**) was carried out in the way described in Sect. 2. Its structure along with the imaginary eigenmode (i1834cm^{-1}) is shown in Fig. 11. Location of H9 more or less half way between N1 and C7 (*cf.* Table 2) is the characteristic feature of this transition state. The energy barrier ΔE=42.37 kcalmol^{-1} that has to be overstepped, corresponds to ΔG value of *ca.* 38 kcalmol^{-1}. It is two times higher than that for the CO_2 detachment. This seems to be mostly due to the high strain within the 4-membered ring formed in the **TS4a** transition state. Thus, this step of the decarboxylation process, though spontaneous from the thermodynamic point of view, is expected to be much slower than the former one.

An alternative mechanism involves two molecules of **4a**. The B3LYP calculations show, that they are capable of forming a relatively stable dimer possessing the C_2 symmetry. It is depicted on Fig. 12a; the binding energy, counterpoise (CP) corrected for the basis set superposition error [28] and ZPE corrected, is equal to 4.26 kcalmol^{-1}. The transition state, corresponding to the imaginary frequency of i1281 cm^{-1}, was found to be only 14.58 kcal mol^{-1} above the dimer (the ZPE corrected value; the corresponding ΔG value is 11.41 kcalmol^{-1}). Analysis of the imaginary eigenmode shows that this is the transition state for the migration of the H9 atom from N1 atom of one **4a** molecule to the C7 atom of the other **4a** molecule (actually, two molecules of **5a** were finally obtained by following the reaction path along the intrinsic reaction coordinate). The B3LYP energetic effect of the overall reaction, *i.e.*, $(\mathbf{4a})_2 \rightarrow 2\ \mathbf{5a}$, is 10.85 kcalmol^{-1} per molecule (ΔG=17.14 kcalmol^{-1}). However, it should be noted that the dimer predicted by B3LYP calculations is stabilized by the interactions of the NH fragment of one molecule (a rather weak dipole) with the non-polar C···C···C system of the other molecule (the quadrupole, *cf.* Fig. 12a). Thus, the

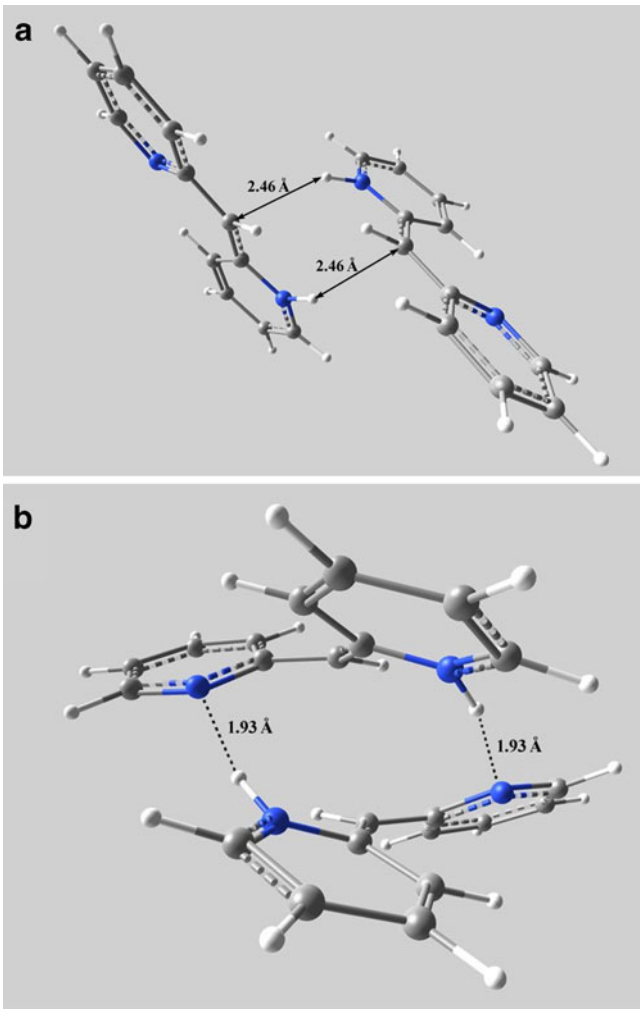

Fig. 12 The dimers of **4a** predicted at (**a**) B3LYP and (**b**) MP2 levels

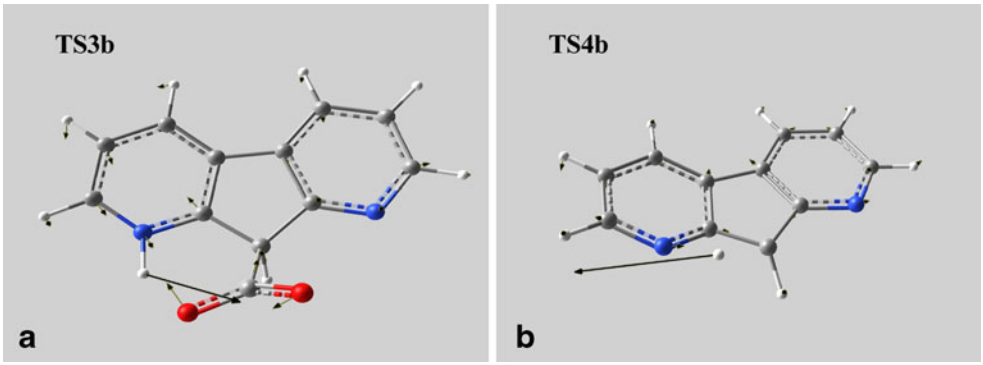

Fig. 13 Transition states **TS3b** and **TS4b**. The arrows show the atomic displacement corresponding to the imaginary frequencies

dispersive-type interactions that show the $U_{disp} \sim r^{-6}$ dependence on distance, are not negligible as compared to the weak electrostatic dipole-quadrupole interactions $U_{dip\text{-}quad} \sim r^{-4}$. The same type of interactions are expected in the transition state. Since DFT is known to poorly describe the dispersive interactions, we decided to investigate this problem using the MP2 method with the same basis set. The geometry optimization of the dimer of **4a** was carried out at the MP2/6-311G** level, using the B3LYP structure as an initial guess. This time we did not obtain the analogous dimer; two NH···N hydrogen bonds were formed instead. This complex, for which the CP corrected binding energy is 14.29 kcalmol^{-1} (the MP2 frequencies were not calculated for practical reasons, but the ZPE estimate obtained at the DFT level, would further reduce this value by *ca.* 0.7 kcalmol^{-1}), is shown in Fig. 12b. Thus it seems, that the DFT calculations overestimate the dispersive interactions when two molecules of **4a** approach each other.

In a view of the MP2 results we conclude that the unimolecular mechanism is responsible for the formation of **5a**. Note that the NH···N links are typically responsible for the chemical exchange of the labile protons. Actually, compounds **4a** and **5a** were obtained by following the reaction path from **TS4a** along the intrinsic reaction coordinate. It should be noted that the reported energy barrier of *ca.* 40 kcalmol^{-1} is comparable to that found for the **1a**→**TS2a**→**3a** reaction. However, low energy barrier of the CO_2 detachment, and significantly higher stability of **5a** as compared to **3a**, proves that synthesis of **1a** [10] could not be successful: this compound spontaneously decarboxylates when it is formed.

Structures of the **TS3b** and **TS4b** transition states in decarboxylation of **1b** as well as imaginary eigenmodes (corresponding to frequencies equal to *i*332cm^{-1} and *i*2050cm^{-1}, respectively) are depicted in Fig. 13. Weaker intramolecular hydrogen bond in **1b** as compared to that in **1a** (*cf.* Table 1), is to some extent responsible for the lower energy barrier ($\Delta G \approx 13$ kcalmol^{-1}, *cf.* Fig. 9) of the dissociation process **1b**→**4b**+CO_2, and for the formation of the N1H bond in **4b**. This stage of the reaction is expected to be spontaneous as well: energy lowering ($\Delta E = -4.8$ kcalmol^{-1}, and $\Delta G = -17.24$ kcalmol^{-1}) was observed. The most significant difference between this (**b**) and previous (**a**) decarboxylation processes is an increase of the energy barrier associated with the migration of H9 toward C7 in the **4b**→**5b** tautomerization by more than 20 kcalmol^{-1}. This value refers to both ΔE and ΔG. Note, that we assume the unimolecular mechanism of tautomerization, in spite of finding a relatively stable dimer of **4b** at the B3LYP level, analogous to the dimer of **4a**, for which the CP corrected binding energy is equal to *ca.* 6 kcalmol^{-1} (the imaginary eigenmode for the transition state found for $(\mathbf{4b})_2 \rightarrow 2$ **5b** reaction corresponds to *i*1149cm^{-1}, the $\Delta E/\Delta G$ energy barriers are *ca.* 14.7/12.6 kcalmol^{-1}, and the $\Delta E/\Delta G$ energetic effects are ca. 7.5/13.6 kcalmol^{-1} per molecule, respectively). However, this time the lengthy MP2 calculations were not carried out. The reason for this can be easily understood when structures involved in the described processes are analyzed. The change in the hybridization of C7 to sp^3 when going from **4b** to **5b** *via* **TS4b** is associated with breaking of the planar symmetry of **4b**. Similar behavior is also observed in reaction **4a**→**5a**. One should keep in mind, however, that the C3C3′ bond

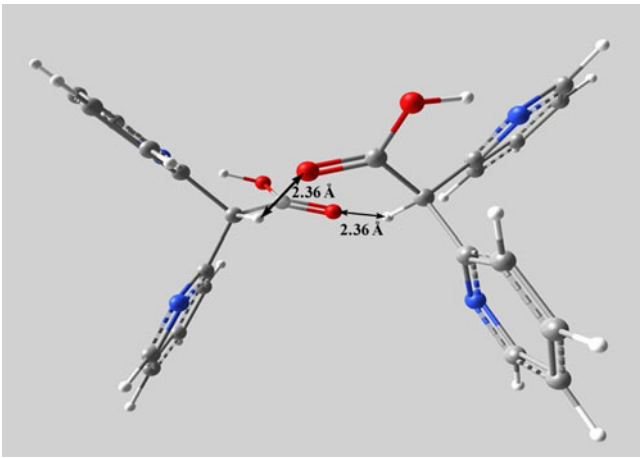

Fig. 14 The dimer of **1a** predicted at B3LYP level

makes the molecules **4b** and **5b** rigid (*cf.* Sect. 3.1), and this results in a steeper energy increase under torsional distortions. As a consequence, significantly risen energy barrier of the **4b**→**5b** step (*ca.* 60 kcal mol^{-1}) may preclude tautomerization to proceed. Thus, **4b** may appear to be the final product of decarboxylation of **1b**. In addition, it can be seen from Fig. 9 and Table 3 that although **5b** is thermodynamically more stable than **5a**, kinetic control of the **4a**→**5a** process is more distinct than that of **4b**→**5b**.

Finally we would like to point out that the bimolecular mechanism was also considered in the case of the enolization process of **1a**. The stable dimer, that could initiate the H proton transfer from C7 atom of one molecule of **1a** to O10 atom of the other molecule of **1a**, was found at the B3LYP level. It is shown in Fig. 14. This time no transition state associated with such a migration was found (the MP2 calculations were not carried out).

Conclusions

Tautomerization and decarboxylation of 2,2-di(pyridin-2-yl)acetic acid were considered to be responsible for its instability. DFT/B3LYP/6-311G** calculations show that the products of decarboxylation of this acid and its rigid cyclic analogue, 1,8-diazafluorene-9-carboxylic acid, are more energetically favorable than the corresponding ene-1,1-diols (products of migration of the methine proton toward the carbonyl oxygen atom) and enaminones (products of migration of the same proton toward the pyridine nitrogen atom). The later tautomers were found to be thermodynamically more stable than enediols. Aromatization of the five membered ring has no effect on stabilization of ene-1,1-diol of 1,8-diazafluorene-9-carboxylic acid. Detachment of CO_2 from 2,2-di(pyridin-2-yl)acetic and 1,8-diazafluorene-9-carboxylic acids to give (*E*)-2-(pyridin-2(1*H*)-ylidenemethyl)pyridine and its cyclic analogue, respectively, may be followed by tautomerization of these by-products into (dipyridin-2-yl)methane and 1,8-diazafluorene. The calculated energy barriers for the CO_2 detachment correspond to quanta of IR radiation, so they can be easily overstepped in the course of reactions expected to afford 2,2-di(pyridin-2-yl)acetic and 1,8-diazafluorene-9-carboxylic acids. Thus, spontaneous decarboxylation of the former is in line with the unsuccessful synthetic efforts.

Despite their instability, the labile compounds may appear as the intermediates in numerous (bio)chemical processes. Conclusions of the present paper may be valid also for other substituted acetic acids (and their homologues) that carry electronegative heteroatoms in the *gamma* positions, such as diacylacetic acids and their derivatives (to be also known as unstable compounds).

References

1. Frey J, Rappoport Z (1996) J Am Chem Soc 118:5169–5181
2. Allen BM, Hegarty AF, O'Neill P, Nguyen MT (1992) J Chem Soc Perkin Trans 2:927–934
3. O'Neill P, Hegarty AF (1987) J Chem Soc Chem Commun 744-745
4. Allen BM, Hegarty AF, O'Neill P (1997) J Chem Soc Perkin Trans 2:2733–2736
5. Urwyler B, Wirz J (1990) Angew Chem Int Ed Engl 29:790–792
6. Gilli G, Belluci F, Ferretti V, Bertolasi V (1989) J Am Chem Soc 111:1023–1028
7. Bertolasi V, Gilli P, Ferretti V, Gilli G (1991) J Am Chem Soc 113:4917–4925
8. Gilli P, Bertolasi V, Ferretti V, Gilli G (1994) J Am Chem Soc 116:909–915
9. Bertolasi V, Gilli P, Ferretti V, Gilli G (1996) Chem Eur J 2:925–934
10. Eistert B, Schade W (1958) Chem Ber 91:1411–1415
11. Taylor PJ (1972) J Chem Soc Perkin Trans 2:1077–1086
12. Sicinska D, Lewandowicz A, Vokal B, Paneth P (2001) J Org Chem 66:5534–5536
13. Katritzky AR, Pozharsky AF (2000) Handbook of Heterocyclic Chemistry, 2nd edn. Pergamon, Elsevier, Amsterdam
14. von Doering WE, Pasternak VZ (1950) J Am Chem Soc 72:143–147
15. Sicinska D, Truhlar DG, Paneth P (2001) J Am Chem Soc 123:7683–7686
16. Headley GW, O'Leary MH (1990) J Am Chem Soc 112:1894–1896
17. Marlier JF, O'Leary MH (1986) J Am Chem Soc 108:4896–4899
18. Panizzon L (1944) Helv Chim Acta 27:1748–1756
19. O'Leary MH (1988) Acc Chem Res 21:450–455, and papers cited therein
20. British Patents 1,099,389; 1,121,922; 1.139,940; 1,147,068 and 1,164,510.
21. Parr RG, Yang W (1989) Density-Functional Theory of Atoms and Molecules. Oxford University Press, New York
22. Becke AD (1993) J Chem Phys 98:5648–5652
23. Lee C, Yang W, Par RG (1993) Phys Rev B 37:785–769
24. Krishnan R, Binkley JS, Seeger R, Pople JA (1980) J Chem Phys 72:650–654
25. Fukui K (1970) J Phys Chem 74:4161–4163
26. Baker J, Wolinski K, Malagoli M, Kinghorn D, Wolinski P, Magyarfalvi G, Saebo S, Janowski T, Pulay P (2009) J Comput Chem 30(2):317–335
27. PQS version 3.3, Parallel Quantum Solutions; 2013 Green Acres Road, Fayetteville, AR 72703, USA
28. Boys SF, Bernardi F (1970) Mol Phys 19:553–566